Supplementary Materials for

Mitigated front contact energy barrier for efficient and stable perovskite solar cells

Daoyong Zhang[1‡], Biao Li[1‡], Pengjie Hang[1], Jiangsheng Xie[3], Yuxin Yao[1], Chenxia Kan[1], Xuegong Yu[1,2*], Yiqiang Zhang[4], Deren Yang[1,2*]

[1]State Key Laboratory of Silicon and Advanced Semiconductor Materials and School of Materials Science and Engineering, Zhejiang University, Hangzhou, 310027, China

[2]ZJU-Hangzhou Global Scientific and Technological Innovation Center, Hangzhou, 311200, China

[3]School of Materials and State Key Laboratory of Optoelectronic Materials and Technologies, Sun Yat-sen University, Shenzhen, 518107, China

[4]School of Materials Science and Engineering, Zhengzhou University, Zhengzhou 450001, China

[‡]These authors contributed equally.

*Corresponding Authors: E-mail: yuxuegong@zju.edu.cn; mseyang@zju.edu.cn

MATERIALS AND METHODS

Materials

The materials and reagents used in this study were obtained from Sigma-Aldric h, except for those specifically mentioned below. Lead iodide (PbI_2, 99.99%), Methylammonium chloride (MACl, 99.9%), phenethylammonium iodide (PEAI), 2,2′,7,7′-Tetrakis[N,N-di(4-methoxyphenyl)amino]-9,9′-spirobifluorene (spiro-OMeT AD) were all purchased from Xi'an Yuri Solar Co., Ltd. For the synthesized Sn O_2 precursor, 1015 mg $SnCl_2 \cdot 2H_2O$, and 335 mg $SnCl_2 \cdot 2H_2O$ were dissolved in 30 mL deionized water in an open beaker. The solution was stirred at room temperature under an oxygen atmosphere until it turned into a light-yellow clea r liquid. Formamidinium iodide (FAI) was purchased from TCI. ITO substrates were purchased from Advanced Election Technology Co., Ltd.

Perovskite solar cells fabrication

The 15 × 15 mm^2 ITO glasses were successively sonicated in deionized water, ethanol, acetone, and isopropanol for 5 min each. The substrates were dried using a hair dryer and cleaned under UV-ozone for 15 min. The ITO surface was coated with an Al_2O_3 layer using atomic layer deposition (ALD, KE-MICRO, PE ALD-F50R) and its thickness was precisely regulated by varying the number of deposition cycles. Al_2O_3 layer was deposited by ALD with 10 cycles (chamber at 130℃, trimethylaluminium (TMA) source with 0.02 s pulse and 45 s purge and H_2O with 0.02 s pulse and 60 s purge, 30 sccm carrier gas of N_2). The substrate undergoes a 15-min UV-ozone cleaning process before electron transport layer deposition. For target, the synthesized SnO_2

precursor solution was spin-coated onto the Al_2O_3 at 3000 rpm for 30 s, and the resulting SnO_2 layer was obtained by heating the sample in air at 180°C for 30 minutes. For control, the SnO_2 layer was deposited directly on the ITO by the same process.

For $FAPbI_3$ (FA, formamidinium) perovskite films fabrication, 461 mg of PbI_2 was dissolved in 900 μL N, N-dimethylformamide (DMF) and 100 μL dimethyl sulfoxide (DMSO). 50 μL precursor solution was spin-coated onto SnO_2 at 1500 rpm for 30 s and then heated at 70°C for 1 minute. Subsequently, a solution comprising of FAI (90 mg) and MACl (9 mg) in 1 ml of isopropanol and then 70 μl of the resulted solution was spin-coated onto the PbI_2 films at a spinning rate of 1750 rpm for 30 s. The perovskite films were removed from a nitrogen-filled glove box and transferred to the ambient air for annealing at 150°C for 15 minutes.

For 1.68 eV perovskite films fabrication, 484 mg of PbI_2, 165.2 mg of $PbBr_2$ and 27.8 mg of CsI were dissolved in 900 μL DMF and 100 μL DMSO. 50 μL precursor solution was spin-coated onto SnO_2 at 1500 rpm for 30 s and then heated at 70°C for 1 minute. Subsequently, a solution comprising of FAI (77 mg), MABr (9.4 mg) and MACl (6.8 mg) in 1 ml of isopropanol and then 70 μl of the resulting solution was spin-coated onto the PbI_2 films at a spinning rate of 1750 rpm for 30 s. The perovskite films were removed from a nitrogen-filled glove box and transferred to the ambient air for annealing at 150°C for 15 minutes.

Following the formation of the perovskite film, it was transferred into a nitrogen-filled glove box. Subsequently, 50 μL 1 mg mL^{-1} PEAI was spin-coated onto the perovskite film at a spinning rate of 5000 rpm for 30 s. For the hole transport layer, 28.75 μL Li-

TFSI acetonitrile solution (520 mg mL^{-1}) and 28.75 μL TBP were added into 72.25 mg mL^{-1} Spiro-OMeTAD chlorobenzene solution. The 40 μL filtered HTL solution using a 0.22 μm PTFE filter was spin-coated onto the PEAI layer at 3000 rpm for 30 s. Finally, a 70 nm thick Au layer was thermally evaporated on top of the Spiro-OMeTAD layer by thermal evaporation with a vacuum less than 1.0×10^{-3} Pa.

For 1cm^2 of $FAPbI_3$ (FA, formamidinium) perovskite films fabrication, 25 × 25 mm^2 ITO glasses were cleaned as previously described. The deposition of Al_2O_3 and the preparation of SnO_2 were consistent with the methods previously described. During the preparation of perovskite films, the volume of PbI_2 was adjusted from 50 μl to 80 μl, and the quantity of FAI: MACl (90 mg: 9 mg in 1 ml IPA) was increased from 70 μl to 100 μl. For PEAI and Spiro-OMeTAD, the volumes were increased to 80 μl and 70 μl, respectively. The other steps are no different from the above.

For Schottky junction device, the doped Spiro-OMeTAD was spin-coated on ITO at 3000 rpm for 30 s. For a metal oxide semiconductor (MOS) device, 150 cycles of Al_2O_3 were deposited on the ITO surface using ALD. Then the doped Spiro-OMeTAD was spin-coated on Al_2O_3 at 3000 rpm for 30 s. Finally, a 70 nm thick Au layer was thermally evaporated on top of the Spiro-OMeTAD layer by thermal evaporation with a vacuum less than 1.0×10^{-3} Pa.

Film and device characterization

The XRD patterns of perovskite were acquired using a D8 Discover X-ray diffractometer (Bruker) equipped with Cu Kα radiation. The morphology of SnO_2 and perovskite was observed using a Hitachi S4800 (Hitachi) Field-Emission Scanning

Electron Microscope (FESEM). X-ray photoelectron spectroscopy characterization was performed using a Kratos AXIS Supra X-ray photoelectron spectrometer with monochromatic Al Kα X-ray (1486.6 eV). Uaviolet photoelectron spectra (UPS) measurements were carried out on a Thermo-Fisher ESCALab Xi+ system. Steady-state PL and time-resolved PL spectra were measured by a FLS980 spectrometer. For femtosecond transient absorption (TA) spectroscopy, the fundamental light beam with a wavelength of 1030 nm output by an Yb:KGW laser (Pharos, Light Conversion Ltd.) operating at 100 KHz was separated to several light beams. The pump beam was generated by a non-collinear optical parametric amplifier. The probe beam was generated by focusing the 1030 nm within a YAG crystal. Both pump and probe pulses were focused and spatially overlapped in the sample space, with the temporal delay between them given by a high-resolution delay stage (Newport). The pumping light is 470 nm at the power of 3 μW. The area of the laser spot is 1~3 μm^2. The current density–voltage (*J–V*) curves were determined using a Keithley 2400 source measurement unit under a simulated AM 1.5G spectrum with a Newport 94022A solar simulator. The light intensity was calibrated by a standard Si reference solar cell (PVM937, Newport) with KG5 filter calibrated by Newport Corporation TAC-PV Lab. The spectral mismatch correction factor is $M = 0.994 \pm 0.001$. The *J–V* curves of devices were measured both in reverse scan (1.2V to 0 V with a step of 0.013 V and a dwelling time of 10 ms at each step) and forward scan (0 V to 1.2 V with a step of 0.013 V and a dwelling time of 10 ms at each step). The device was tested at room temperature (25 ± 5 ℃) with a relative humidity of 30 ± 10% under ambient conditions. All devices were

measured without pre-conditioning such as light-soaking the device. The device was tested with a calibrated mask with an aperture area of 0.0528 cm^2. The steady-state PCE was calculated by measuring the stabilized photocurrent density under a constant bias voltage. EQE curves were measured using an EQE measurement system (Model QEX10, PV Measurements, Inc.) across a functional wavelength from 300 to 1000 nm. The stability tests were carried in a nitrogen glove-box under a 1-sun-equivalent light-emitting diode lamp. The testing temperature is 25 ± 5 ℃. The capacitance measurement (Keysight E4980A) is tested via an AC frequency of 40 kHz and voltage of 20 mV.

Supplementary Note

Calculation of the density of fixed charges

The density of fixed charges is calculated based on the Gauss' law. For a pair of charged plates, the surface density of fixed charges (σ) can be described by

$$\sigma = \frac{E}{\varepsilon_0 \varepsilon_r} \tag{S1}$$

where E is the electric field intensity between the charged plates; ε_0 is the vacuum dielectric constant; ε_r is the relative dielectric constant. The E can be calculated by

$$E = \frac{U}{d} \tag{S2}$$

where U is the potential difference generated by the fixed charges; d is the distance between the charged plates. The potential difference is the change of V_{bi} after the insertion of Al_2O_3 into ITO/Spiro-OMeTAD/Au device, which is shown in Fig. 1(a) and (d). Then, the σ can be easily calculated.

Drift-diffusion simulation

We performed drift-diffusion simulations via SCAPS-1D software developed by the group of Prof. Burgelman from Ugent University to evaluate the effects of Φ_{FC} on the performance of PSCs[1]. This software solves the continuity equation for electrons and holes together with the Poisson equation. In the simulation, we constructed a n-i-p PSC with a structure of ITO/SnO_2/Perovskite/Spiro-OMeTAD/Au and the corresponding parameters are provided in the Supplementary Tables 1-3[2,3].

Transient Absorption (TA) analysis

The distribution of photogenerated charge carriers can be accurately described by a one-dimensional diffusion model (Equation S3). This model enables a quantitative analysis of the population of photogenerated carriers over time and at varying depths within the film. The utilized one-dimensional diffusion model, presented below, describes the carrier density, denoted as *N(x,t)*, as a function of the film depth (*x*) and time (*t*). The model parameters include τ_B, the lifetime of photogenerated charge carriers in the bulk, and *D*, the ambipolar diffusion coefficient of charge carriers in the film.

$$\frac{\partial N(x,t)}{\partial t} = D\frac{\partial^2 N(x,t)}{\partial x^2} - \frac{N(x,t)}{\tau_B} \quad \text{S3}$$

Assuming instantaneous carrier generation and within the time resolution of the pump excitation pulse, the initial carrier concentration at the film surface can be determined using

$$N_0 = \alpha(1 - R)J_0 \quad \text{S4}$$

the initial carrier density, denoted as N_0, where α represents the absorption coefficient corresponding to the selected pump wavelength, R denotes the reflectance of the pump, and J_0 is the carrier density determined by the measured power output and measured spot size of the excitation pulse.

To solve the diffusion model, boundary conditions were set with the following conditions:

$$\left.\frac{\partial N(x,t)}{\partial t}\right|_{X=0} = \frac{SRV}{D}N(0,t) \; and \; \left.\frac{\partial N(x,t)}{\partial t}\right|_{X=M} = \frac{SRV}{D}N(M,t) \quad \text{S5}$$

where M is the film thickness and SRV is the surface recombination velocity[4,5].

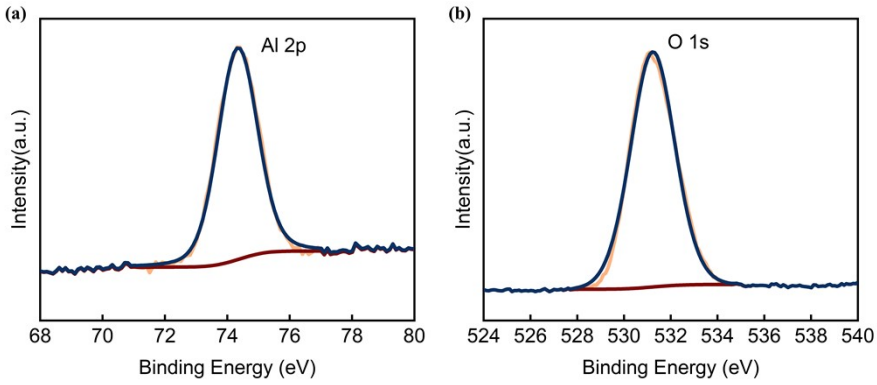

Fig. S1. XPS results of Al_2O_3 layer deposited on ITO substrates.

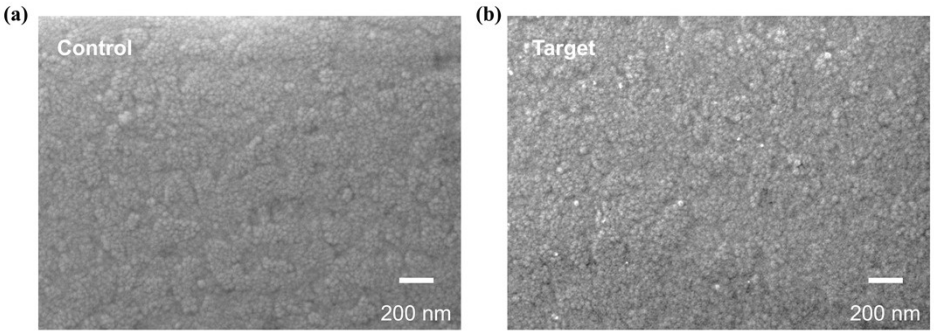

Fig. S2. SEM top-view images of SnO_2 on ITO with and without Al_2O_3.

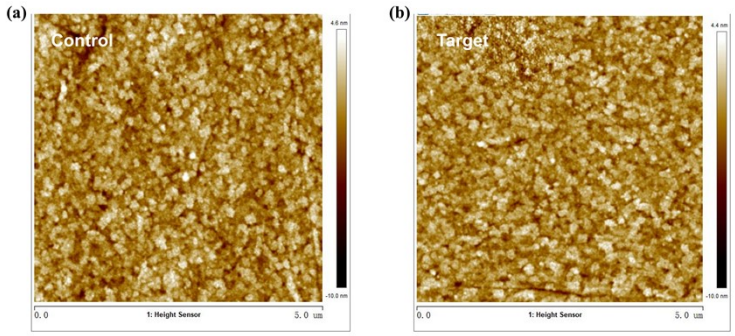

Fig. S3. AFM morphology images of SnO_2 on ITO with and without Al_2O_3.

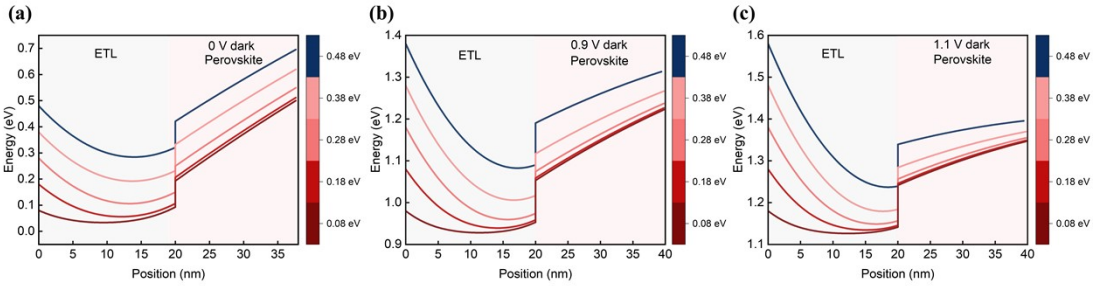

Fig. S4. Energy band simulation results near the ETL/Perovskite heterojunction in PSCs with representative applied forward biases (0 V, 0.9 V, 1.1 V) at dark conditions.

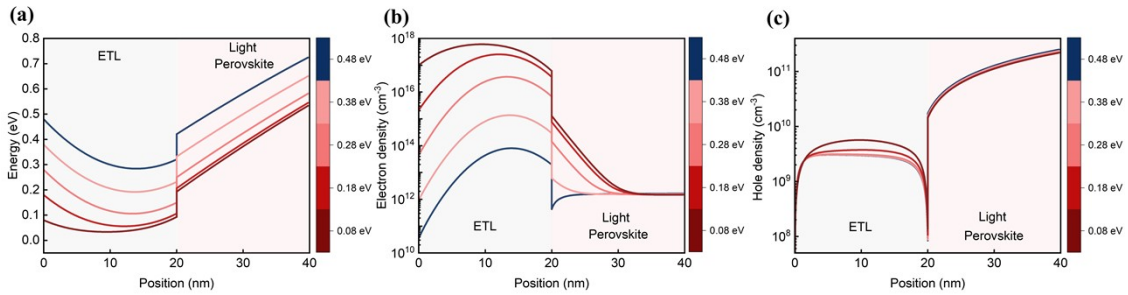

Fig. S5. Simulations of the density distribution of electrons and holes near the ETL/Perovskite heterojunction under illumination.

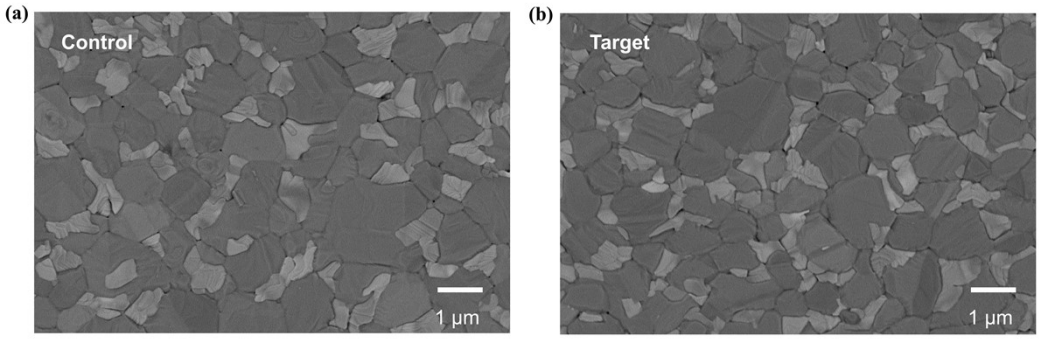

Fig. S6. SEM top-view images of perovskite films deposited on ITO/SnO_2 and ITO/Al_2O_3/SnO_2.

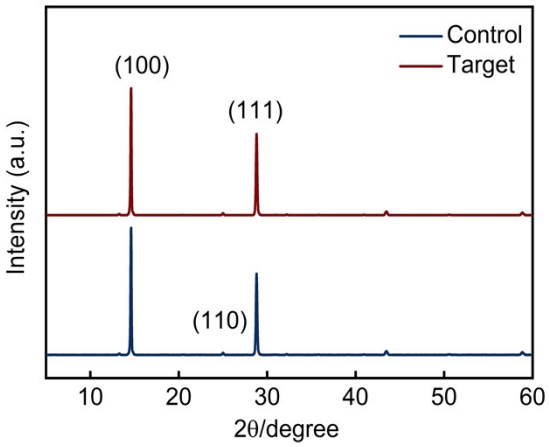

Fig. S7. XRD measurements of control (ITO/SnO_2/perovskite) and the target (ITO/Al_2O_3/SnO_2/perovskite).

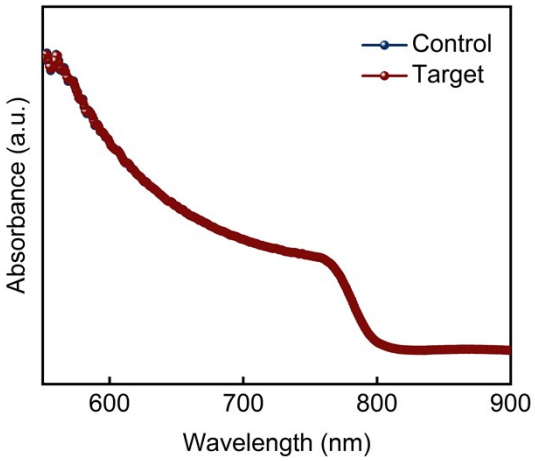

Fig. S8. UV-vis spectra of control (ITO/SnO_2/perovskite) and the target (ITO/Al_2O_3/SnO_2/perovskite).

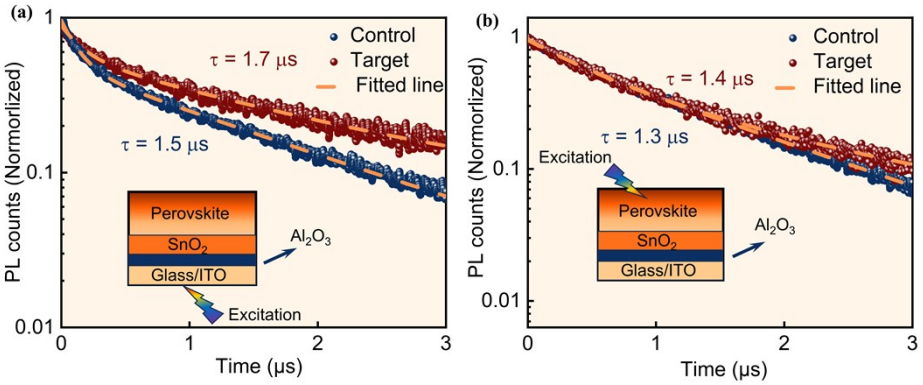

Fig. S9. TRPL decays of perovskites deposited on ITO/SnO_2 and ITO/Al_2O_3/SnO_2 with different incident directions: glass side and perovskite side.

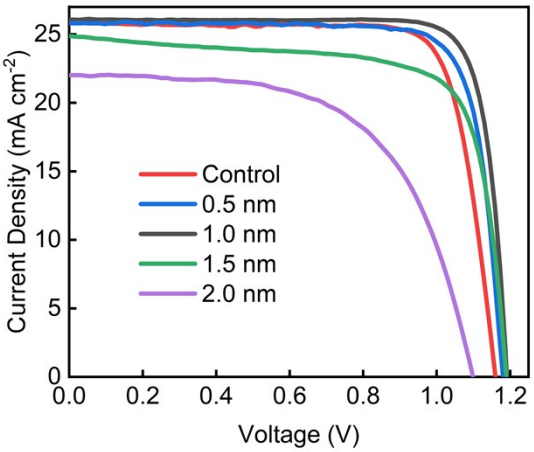

Fig. S10. The typical *J-V* curves of the devices with different thicknesses of Al_2O_3.

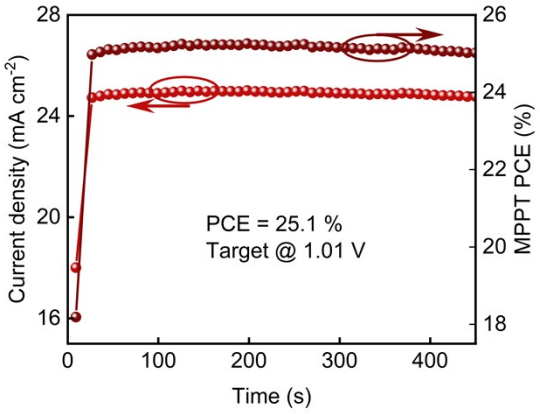

Fig. S11. Steady-state output at maximum power point of the target device.

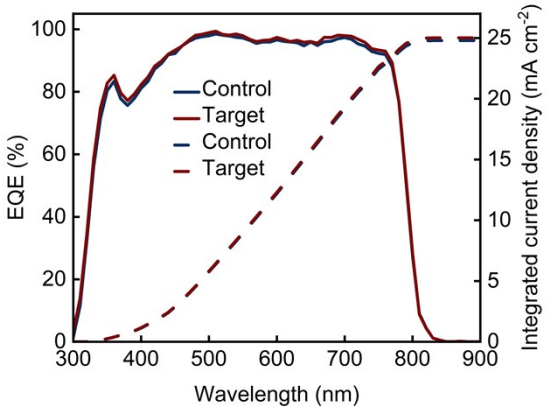

Fig. S12. External quantum efficiency (EQE) and integrated current density of control and target devices.

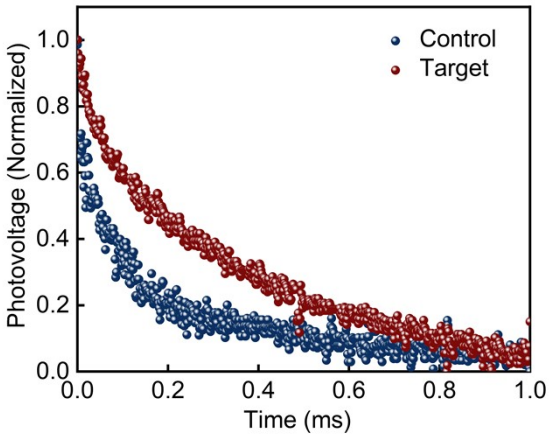

Fig. S13. Transient photovoltage (TPV) decay of control and target devices.

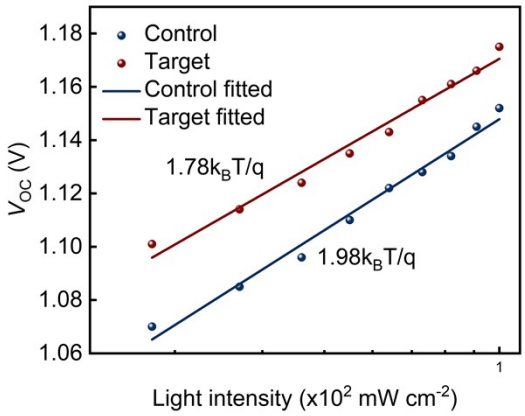

Fig. S14. Light intensity dependent V_{OC} tests.

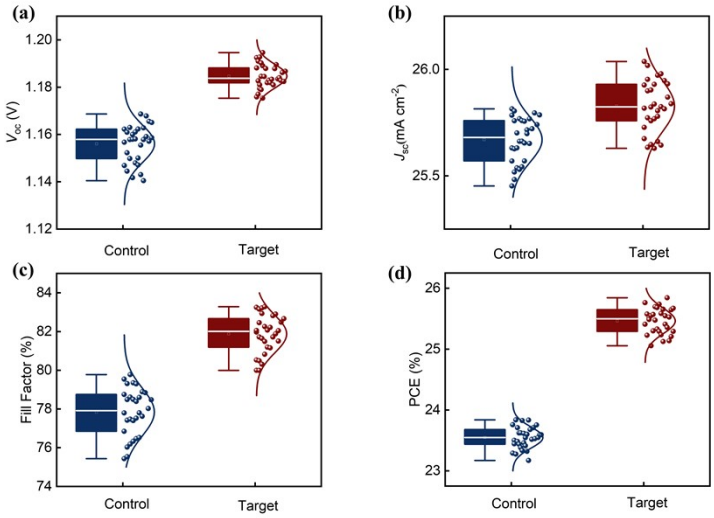

Fig. S15. Box plots of the **A**, V_{oc}, **B**, J_{sc}, **C**, FF, **D**, PCE for the control and the target devices.

Test and Calibration Center of New Energy Device and Module,
Shanghai Institute of Microsystem and Information Technology,
Chinese Academy of Sciences (SIMIT)

Measurement Report

Report No. 23TR090404

Client Name	Zhejiang University
Client Address	No. 38 Zheda Road, West Lake District, Hangzhou,Zhejiang
Sample	Perovskite Solar Cell
Manufacturer	Zhejiang University
Measurement Date	4th September, 2023

Performed by:	Qiang Shi Qiang Shi	**Date:** 04/09/2023
Reviewed by:	Wenjie Zhao Wenjie Zhao	**Date:** 04/09/2023
Approved by:	Yucheng Liu Yucheng Liu	**Date:** 04/09/2023

Address: No.235 Chengbei Road, Jiading, Shanghai **Post Code:**201800
E-mail: solarcell@mail.sim.ac.cn **Tel:** +86-021-69976921

Sample Information	
Sample Type	Perovskite solar cell
Serial No.	13-1-1#
Lab Internal No.	23090401-4#
Measurement Item	I-V characteristic
Measurement Environment	24.5±2.0°C, 53.5±5.0%R.H

Measurement of I-V characteristic	
Reference cell	PVM 1121
Reference cell Type	mono-Si, WPVS, calibrated by NREL (Certificate No. ISO 2075)
Calibration Value/Date of Calibration for Reference cell	144.53mA/ Feb. 2023
Measurement Conditions	Standard Test Condition (STC): Spectral Distribution: AM1.5 according to IEC 60904-3 Ed.3, Irradiance: 1000±50W/m², Temperature: 25±2°C
Measurement Equipment/ Date of Calibration	AAA Steady State Solar Simulator (YSS-T155-2M) / July.2023 IV test system (ADCMT 6246) / June. 2023 Measuring Microscope (MF-B2017C) / July.2023
Measurement Method	I-V Measurement: Dual-lamp solar simulator spectral distribution adjusted to mask the match factor within 1.00±0.02; Irradiance adjusted to 1000W/m² according to the short circuit current value of calibrated reference cell; Logarithmic sweep in both directions (Isc to Voc and Voc to Isc) during one flash based on IEC 60904-1:2020.
Measurement Uncertainty	Area: 1.0% (k=2); Isc: 2.1% (k=2); Voc: 1.0% (k=2); Pmax: 2.5% (k=2); Eff: 2.6% (k=2)

Report No. 23TR090404

====Measurement Results ====

	Forward Scan (Isc to Voc)	Reverse Scan (Voc to Isc)
Area	0.0528 cm^2	
Isc	1.376 mA	1.372 mA
Voc	1.175 V	1.178 V
Pmax	1.307 mW	1.334 mW
Ipm	1.301 mA	1.307 mA
Vpm	1.004 V	1.020 V
FF	80.81 %	82.51 %
Eff	24.74 %	25.27 %

- Designated illumination area defined by a mask was measured by a measuring microscope.
- Test results listed in this measurement report refer exclusively to the mentioned test sample.
- The results apply only at the time of the test, and do not imply future performance.

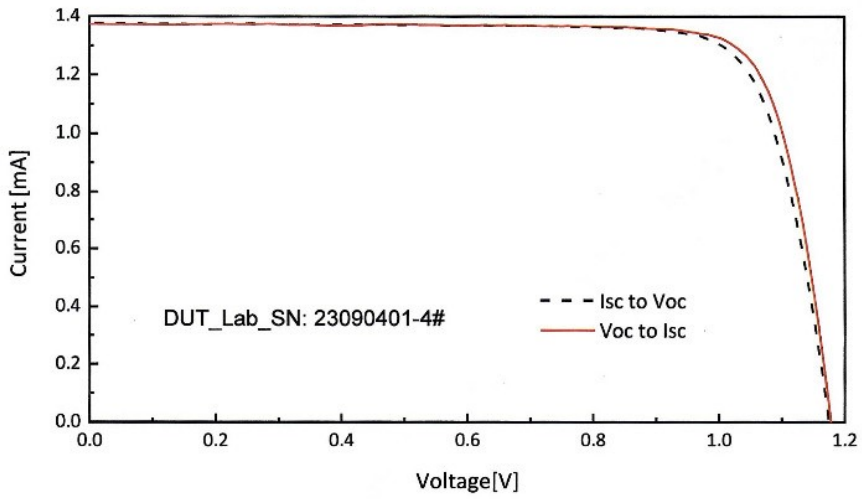

Fig.1 I-V curves of the measured sample

-------End of Report-------

3 / 3

Fig. S16. Certification of the small-area device with Al_2O_3 by Shanghai Institute of Microsystem and Information Technology (SIMIT), Chinese Academy of Sciences.

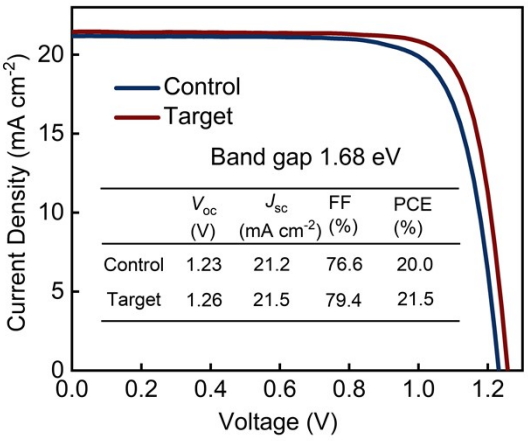

	V_{oc} (V)	J_{sc} (mA cm^{-2})	FF (%)	PCE (%)
Control	1.23	21.2	76.6	20.0
Target	1.26	21.5	79.4	21.5

Fig. S17. *J-V* curves of control and target devices using 1.68 eV perovskite.

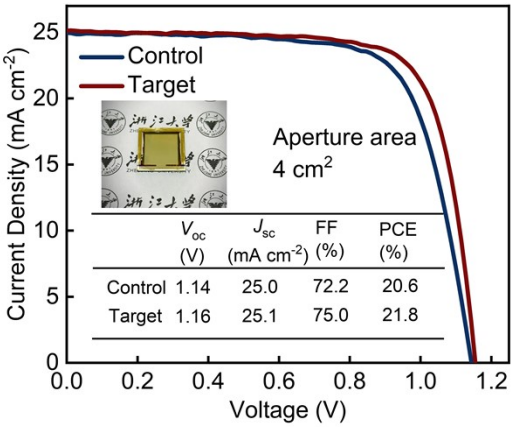

	V_{oc} (V)	J_{sc} (mA cm^{-2})	FF (%)	PCE (%)
Control	1.14	25.0	72.2	20.6
Target	1.16	25.1	75.0	21.8

Fig. S18. *J-V* curves of PSCs with and without Al_2O_3 with an active area of 4 cm^2.

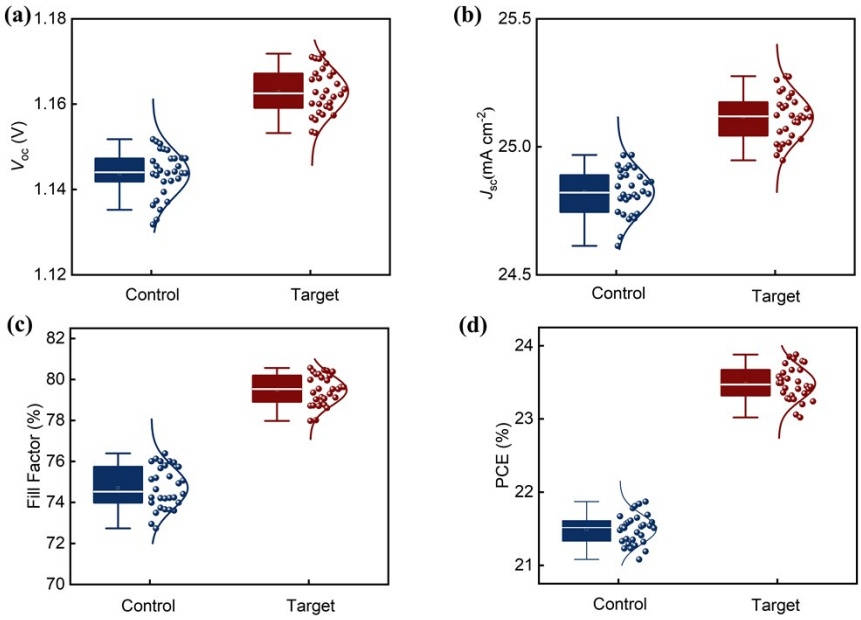

Fig. S19. Photovoltaic parameters for 30 PSCs with and without Al_2O_3 with an active area of 1 cm^2.

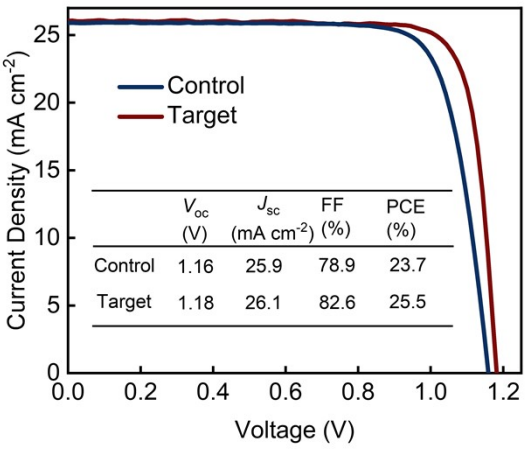

	V_{oc} (V)	J_{sc} (mA cm^{-2})	FF (%)	PCE (%)
Control	1.16	25.9	78.9	23.7
Target	1.18	26.1	82.6	25.5

Fig. S20. *J-V* curves of the PSCs based on FTO with and without Al_2O_3.

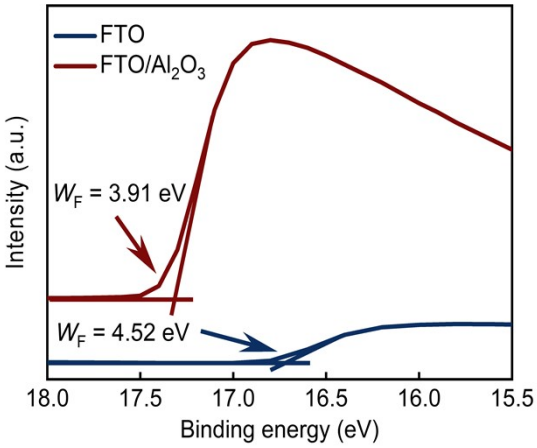

Fig. S21. UPS results of ITO samples with and without Al_2O_3.

Table S1. The statistics of the W_F of SnO_2 fabricated by sol–gel method in literatures.

WF of SnO_2 (eV)	Method	Reference
4.36	Sol–Gel Method	[6]
4.05	Sol–Gel Method	[7]
3.77	Sol–Gel Method	[8]
3.96	Sol–Gel Method	[9]
4.17	Sol–Gel Method	[10]
3.96	Sol–Gel Method	[11]
4.22	Sol–Gel Method	[12]
4.34	Sol–Gel Method	[13]
3.84	Sol–Gel Method	[14]

Table S2. The statistics of the W_F of ITO in literatures.

WF of ITO (eV)	Reference
4.78	[15]
4.8	[16]
4.8	[17]
4.7	[18]
4.8	[19]
4.8	[20]
4.8	[21]

Table S3. The statistics of the W_F of FTO in literatures.

WF of FTO (eV)	Reference
4.6	[13]
4.67	[22]
4.7	[23]
4.7	[24]
4.6	[25]
4.7	[26]
4.63	[27]

Table S4. Parameters of the perovskite layer and its interface in the simulations[2].

Parameter	Value [unit]
Relative Permittivity	6.5
Bandgap	1.52 [eV]
Electron Affinity	3.9 [eV]
Effective density of states (valence band)	2.2×10^{18} [cm^{-3}]
Effective density of states (conduction band)	2.2×10^{18} [cm^{-3}]
Electron mobility	0.6 [$cm^2\ V^{-1}\ s^{-1}$]
Hole mobility	0.6 [$cm^2\ V^{-1}\ s^{-1}$]
Acceptor concentration	5.2×10^{16} [cm^{-3}]
Carrier diffusion length	2.8 [μm]
Interface recombination velocity (SnO_2/Perovskite)	50 [$cm\ s^{-1}$]
Thickness	1000 [nm]

Table S5. Parameters of the SnO_2 layer in the simulations[3].

Parameter	Value [unit]
Relative Permittivity	9
Bandgap	3.2 [eV]
Electron Affinity	4.0 [eV]
Effective density of states (valence band)	2.2×10^{18} [cm^{-3}]
Effective density of states (conduction band)	1×10^{19} [cm^{-3}]
Electron mobility	100 [$cm^2\ V^{-1}\ s^{-1}$]
Hole mobility	0.256 [$cm^2\ V^{-1}\ s^{-1}$]
Donor concentration	1.0×10^{18} [cm^{-3}]
Thickness	20 [nm]

Table S6. Parameters of the Spiro-OMeTAD layer in the simulations[3].

Parameter	Value [unit]
Relative Permittivity	3
Bandgap	3.0 [eV]
Electron Affinity	2.42 [eV]
Effective density of states (valence band)	1×10^{19} [cm^{-3}]
Effective density of states (conduction band)	1×10^{19} [cm^{-3}]
Electron mobility	2×10^{-4} [$cm^2\ V^{-1}\ s^{-1}$]
Hole mobility	2×10^{-4} [$cm^2\ V^{-1}\ s^{-1}$]
Acceptor concentration	2.0×10^{18} [cm^{-3}]
Thickness	20 [nm]

Table S7. The parameters for the simulated *J-V* curves with different Φ_{FC}.

Φ_{FC} (eV)	V_{OC} (V)	J_{SC} (mA cm^{-2})	FF (%)	PCE (%)
0.78	1.05	25.26	62.29	16.57
0.68	1.14	25.31	65.29	18.94
0.58	1.15	25.35	72.83	21.31
0.48	1.12	25.40	82.89	23.65
0.38	1.17	25.44	85.36	25.56
0.28	1.19	25.47	86.26	26.30
0.18	1.20	25.48	86.47	26.52
0.08	1.21	25.50	86.57	26.62

Table S8. Photovoltaic parameters for the PSCs with the configuration ITO/Al_2O_3/SnO_2/Perovskite/PEAI/Spiro/Au.

Al_2O_3 (nm)	V_{OC} (V)	J_{SC} (mA cm^{-2})	FF (%)	PCE (%)
0	1.16	25.8	79.5	23.8
0.5	1.18	25.9	80.1	24.5
1.0	1.19	26.0	83.2	25.7
1.5	1.18	25.1	73.7	21.8
2.0	1.09	22.0	60.2	14.4

References and Notes

1 M. Burgelman, P. Nollet and S. Degrave, *Thin Solid Films*, 2000, **361–362**, 527–532.

2 F. Azri, A. Meftah, N. Sengouga and A. Meftah, *Solar Energy*, 2019, **181**, 372–378.

3 S. Boumaza, B. Bellal, A. Boudjemaa and M. Trari, *Solar Energy*, 2016, **139**, 444–451.

4 Y. Yang, Y. Yan, M. Yang, S. Choi, K. Zhu, J. M. Luther and M. C. Beard, *Nat. Commun.*, 2015, **6**, 7961.

5 Y. Yang, M. Yang, D. T. Moore, Y. Yan, E. M. Miller, K. Zhu and M. C. Beard, *Nat. Energy*, 2017, **2**, 16207.

6 Q. Jiang, L. Zhang, H. Wang, X. Yang, J. Meng, H. Liu, Z. Yin, J. Wu, X. Zhang and J. You, *Nat. Energy*, 2016, **2**, 1–7.

7 D. Yang, R. Yang, K. Wang, C. Wu, X. Zhu, J. Feng, X. Ren, G. Fang, S. Priya and S. (Frank) Liu, *Nat. Commun.*, 2018, **9**, 3239.

8 S. S. Mali, J. V. Patil, J.-Y. Shao, Y.-W. Zhong, S. R. Rondiya, N. Y. Dzade and C. K. Hong, *Nat. Energy*, 2023, **8**, 989–1001.

9 Y. Wang, M. Feng, H. Chen, M. Ren, H. Wang, Y. Miao, Y. Chen and Y. Zhao, *Adv. Mater.*, 2024, **36**, 2305849.

10 J.-H. Kim, Y. R. Kim, J. Kim, C.-M. Oh, I.-W. Hwang, J. Kim, S. Zeiske, T. Ki, S. Kwon, H. Kim, A. Armin, H. Suh and K. Lee, *Adv. Mater.*, 2022, **34**, 2205268.

11 Z. Liu, K. Deng, J. Hu and L. Li, *Angew. Chem. Int. Ed*., 2019, **131**, 11621–11628.

12 R. Yuan, B. Cai, Y. Lv, X. Gao, J. Gu, Z. Fan, X. Liu, C. Yang, M. Liu and W.-H. Zhang, *Energy Environ. Sci.*, 2021, **14**, 5074–5083.

13 K. Choi, J. Lee, H. I. Kim, C. W. Park, G.-W. Kim, H. Choi, S. Park, S. A. Park and T. Park, *Energy Environ. Sci.*, 2018, **11**, 3238–3247.

14 Z. Liu, L. Qiu, L. K. Ono, S. He, Z. Hu, M. Jiang, G. Tong, Z. Wu, Y. Jiang, D.-Y. Son, Y. Dang, S. Kazaoui and Y. Qi, *Nat. Energy*, 2020, **5**, 596–604.

15 C.-M. Hung, C.-L. Mai, C.-C. Wu, B.-H. Chen, C.-H. Lu, C.-C. Chu, M.-C. Wang, S.-D. Yang, H.-C. Chen, C.-Y. Yeh and P.-T. Chou, *Angew. Chem. Int. Ed*., 2023, **135**, e202309831.

16 Y. Hou, W. Chen, D. Baran, T. Stubhan, N. A. Luechinger, B. Hartmeier, M. Richter, J. Min, S. Chen, C. O. R. Quiroz, N. Li, H. Zhang, T. Heumueller, G. J. Matt, A. Osvet, K. Forberich, Z.-G. Zhang, Y. Li, B. Winter, P. Schweizer, E. Spiecker and C. J. Brabec, *Adv. Mater.*, 2016, **28**, 5112–5120.

17 N. Beaumont, I. Hancox, P. Sullivan, R. A. Hatton and T. S. Jones, *Energy Environ. Sci.*, 2011, **4**, 1708–1711.

18 M. G. Helander, Z. B. Wang, J. Qiu, M. T. Greiner, D. P. Puzzo, Z. W. Liu and Z. H. Lu, *Science*, 2011, **332**, 944–947.

19 Z. Li, X. Sun, X. Zheng, B. Li, D. Gao, S. Zhang, X. Wu, S. Li, J. Gong, J. M. Luther, Z. Li and Z. Zhu, *Science*, 2023, **382**, 284–289.

20 S.-Q. Sun, J.-W. Tai, W. He, Y.-J. Yu, Z.-Q. Feng, Q. Sun, K.-N. Tong, K. Shi, B.-C. Liu, M. Zhu, G. Wei, J. Fan, Y.-M. Xie, L.-S. Liao and M.-K. Fung, *Adv. Mater.*, 2400421.

21 Z.-K. Tan, R. S. Moghaddam, M. L. Lai, P. Docampo, R. Higler, F. Deschler, M. Price, A. Sadhanala, L. M. Pazos, D. Credgington, F. Hanusch, T. Bein, H. J. Snaith and R. H. Friend, *Nat.*

Nanotech., 2014, **9**, 687–692.

22 S. Heo, G. Seo, Y. Lee, D. Lee, M. Seol, J. Lee, J.-B. Park, K. Kim, D.-J. Yun, Y. S. Kim, J. K. Shin, T. K. Ahn and M. K. Nazeeruddin, *Energy Environ. Sci.*, 2017, **10**, 1128–1133.

23 W. Chen, Y. Wu, J. Liu, C. Qin, X. Yang, A. Islam, Y.-B. Cheng and L. Han, *Energy Environ. Sci.*, 2015, **8**, 629–640.

24 Y. Chen, Q. Wang, Y. Yao, J. Yang, W. Tang, W. Qiu, Y. Wu and Q. Peng, *Energy Environ. Sci.*, 2023, **16**, 5243–5254.

25 Z. Wei, K. Yan, H. Chen, Y. Yi, T. Zhang, X. Long, J. Li, L. Zhang, J. Wang and S. Yang, *Energy Environ. Sci.*, 2014, **7**, 3326–3333.

26 W. Chen, F.-Z. Liu, X.-Y. Feng, A. B. Djurišić, W. K. Chan and Z.-B. He, *Adv. Energy Mater.*, 2017, **7**, 1700722.

27 M. Crespo-Quesada, L. M. Pazos-Outón, J. Warnan, M. F. Kuehnel, R. H. Friend and E. Reisner, *Nat. Commun.*, 2016, **7**, 12555.